

Article

# Quantification of the Elastic Moduli of Lumbar Erector Spinae and Multifidus Muscles Using Shear-Wave Ultrasound Elastography

Tae Hyun Lim <sup>1</sup>, Deukhee Lee <sup>2,3</sup> , Olga Kim <sup>1,3</sup>  and Song Joo Lee <sup>1,3,\*</sup>

<sup>1</sup> Center for Bionics, Biomedical Research Institute, Korea Institute of Science and Technology, Seoul 02792, Korea; tuna28@naver.com (T.H.L.); olgakim@kist.re.kr (O.K.)

<sup>2</sup> Center for Healthcare Robotics, AI and Robot Institute, Korea Institute of Science and Technology, Seoul 02792, Korea; dkylee@kist.re.kr

<sup>3</sup> Division of Bio-Medical Science and Technology, KIST School, Korea University of Science and Technology, Seoul 02792, Korea

\* Correspondence: songjoolee@kist.re.kr; Tel.: +82-2-958-5645

**Featured Application:** The findings and approach can potentially be used to guide surgical training and planning for developing a minimal-incision surgical procedure by considering surgical position-dependent muscle material properties.

**Abstract:** Although spinal surgeries with minimal incisions and a minimal amount of X-ray exposure (MIMA) mostly occur in a prone posture on a Wilson table, the prone posture's effects on spinal muscles have not been investigated. Thus, this study used ultrasound shear-wave elastography (SWE) to compare the material properties of the erector spinae and multifidus muscles when subjects lay on the Wilson table used for spinal surgery and the flat table as a control condition. Thirteen male subjects participated in the study. Using ultrasound SWE, the shear elastic moduli (SEM) of the erector spinae and multifidus muscles were investigated. Significant increases were found in the SEM of erector spinae muscle 1, erector spinae muscle 2, and multifidus muscles on the Wilson table (W) compared to in the flat table (F; W:  $22.19 \pm 7.15$  kPa, F:  $10.40 \pm 3.20$  kPa,  $p < 0.001$ ; W:  $12.10 \pm 3.31$  kPa, F:  $7.17 \pm 1.71$  kPa,  $p < 0.001$ ; W:  $18.39 \pm 4.80$  kPa, F:  $11.43 \pm 2.81$  kPa,  $p < 0.001$ , respectively). Our results indicate that muscle material properties measured by SWE can be changed due to table posture, which should be considered in biomechanical modeling by guiding surgical planning to develop minimal-incision surgical procedures.

**Keywords:** erector spinae; multifidus; shear-wave elastography (SWE); Wilson table



**Citation:** Lim, T.H.; Lee, D.; Kim, O.; Lee, S.J. Quantification of the Elastic Moduli of Lumbar Erector Spinae and Multifidus Muscles Using Shear-Wave Ultrasound Elastography. *Appl. Sci.* **2021**, *11*, 1782. <https://doi.org/10.3390/app11041782>

Academic Editor: Alessandro Ramalli

Received: 11 November 2020

Accepted: 11 February 2021

Published: 17 February 2021

**Publisher's Note:** MDPI stays neutral with regard to jurisdictional claims in published maps and institutional affiliations.



**Copyright:** © 2021 by the authors. Licensee MDPI, Basel, Switzerland. This article is an open access article distributed under the terms and conditions of the Creative Commons Attribution (CC BY) license (<https://creativecommons.org/licenses/by/4.0/>).

## 1. Introduction

Over the last decade, there has been a steady shift in spinal surgical techniques toward using minimal incisions and a minimal amount of X-ray exposure (MIMA) to lower blood loss, accelerate patient recovery, and shorten hospital stays [1]. To precisely perform spine surgery with MIMA, it might be necessary to accurately register a patient and an image to develop surgical robots and image-guided navigation systems. Various image-to-patient registration technologies exist on image-guided navigation systems for spinal surgeries [2–6]. Recently, computer navigation was employed as a useful tool to aid in boosting the accuracy of spinal-surgery performance, particularly for the most practiced pedicle screw-placement technique [7–10]. However, outcomes of image-guided robotic spine surgery remain disputable [10]. Among several errors that could be made by robots, deviation in robotic-arm positioning and the trajectory of the robotic drill might be influenced by pressure that occurs while going through tissue [11]. In earlier studies, soft-tissue-related errors in robot-assisted techniques were revealed [12,13]. Therefore, to aid surgical procedures that use MIMA, utilizing aforementioned various image-to-patient

registration technologies on the basis of the surface information of patients' backs might not be enough to accurately estimate the spine location and possible biomechanics that could influence the trajectory of the robotic drill. Without taking numerous X-rays of a patient's various postures during surgery, a biomechanical spine model can simulate multiple possible scenarios with various patient postures that could occur during surgery. Surgical training and planning can be better informed by surgical instrument and position [14,15]. Therefore, generating a biomechanical spine model could be beneficial.

To generate a more accurate biomechanical spinal model, both hard-tissue shape information obtained from computerized-tomography (CT) images, and soft-tissue shape and elasticity information obtained from magnetic resonance imaging (MRI) or ultrasound imaging could be beneficial. However, not many studies include soft-tissue information when creating a biomechanical model. Recently, shear-wave elastography (SWE) was used to investigate musculoskeletal pathologies and conditions because tissue stiffness can be algebraically derived from shear-wave speed in the ultrasound machine [16]. Shear-wave speed is estimated by tissue motion induced by generated shear waves using acoustic radiation force along with an ultrasound probe [17,18]. Although various studies investigated the elastic modulus of soft tissue using SWE, only a few investigated the elastic modulus of medial gastrocnemius muscles at different ankle positions using both SWE and strain elastography. Additionally, little research has been conducted on erector spinae and multifidus muscles at different trunk positions to find an ideal stretching posture using shear-wave ultrasound elastography [19–21]. The elastic modulus of muscles around the spine, such as erector spinae and multifidus, could be different depending on subject and posture. However, the elastic modulus of the erector spinae and multifidus muscles at the prone posture related to spine surgery on a Wilson table has not been investigated. Since spinal surgeries are performed on Wilson tables, it is necessary to investigate whether differences in the elastic modulus of muscles around the spine exist between surgical and resting postures.

Therefore, the goal of this study was to compare skin thickness, muscle thickness, and the elastic modulus of muscles around the lumbar spine, such as erector spinae and multifidus muscles, using shear-wave ultrasound images of the prone posture on a flat table and a Wilson table. We hypothesize that the two postures led to significant differences in the elastic modulus of the erector spinae and multifidus muscles, and skin and muscle thickness.

## 2. Materials and Methods

### 2.1. Subjects

On the basis of our pilot study that measured the shear elastic modulus in the erector spinae muscle, a sample size of 13 was determined (power = 0.8;  $\alpha$  = 0.05; effect size  $d$  = 0.88). Thus, 13 healthy male subjects participated in the study (age,  $26.2 \pm 3.2$  years; body height,  $170.0 \pm 6.5$  cm; body weight,  $64.7 \pm 12.9$  kg). Because there are possible effects of sex hormones on muscle mechanics that contribute to neuromechanical values [22], only male subjects participated in the study. Neck circumference was  $31.2 \pm 8.6$  cm, waist circumference was  $79.6 \pm 5.8$  cm, and thigh circumference was  $49.0 \pm 4.2$  cm. Exclusion criteria for the study were subjects with neurological and orthopedic disorders. All subjects gave written informed consent, and the experimental procedure was approved by the Institutional Review Board of the Korea Institute of Science and Technology (KIST) prior to the experiment.

### 2.2. Spinal-Alignment Measurement

Sagittal spinal alignments, specifically thoracic- and lumbar-curvature angles, were measured at each prone posture on the flat and the Wilson table (Figure 1) using the Acumar Single Digital Inclinator (Lafayette Instrument Company, Lafayette, US). Before measurements, the spinous processes of the first thoracic vertebrae (T1), 12th thoracic vertebrae (T12), and 5th lumbar vertebrae (L5) were palpated and marked. Then, the

dial on the inclinometer was set to zero, and measured values at each spine level were recorded. The zero value on the inclinometer was perfectly horizontal. A negative value meant that the inclinometer tilted forward, and a positive value meant that the inclinometer tilted backward.

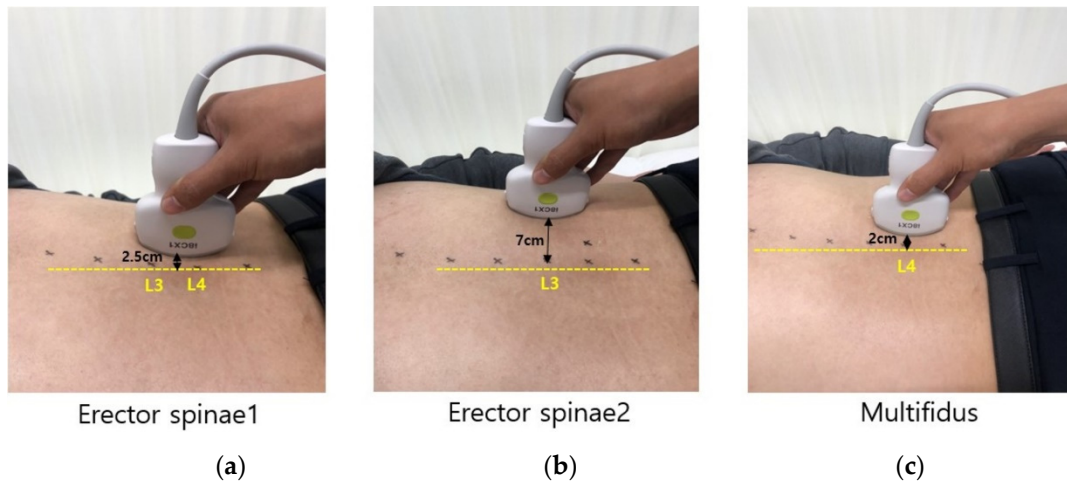


**Figure 1.** Location of ultrasound probe to measure skin thickness, muscle thickness, and shear-wave elastography (SWE). (a) Erector spinae 1; (b) erector spinae 2; and (c) multifidus.

### 2.3. Ultrasound Measurement

Ultrasound imaging device Aplio i700 (Canon Medical Systems, Tochigi, Japan) was used to measure skin and muscle thickness, and to quantify the modulus of elasticity of a lumbar erector spinae and multifidus muscle. A convex i8CX1 probe with a 5.5 MHz central frequency was used for collecting SWE images. The convex probe was used because of the curved shape of the multifidus muscle [23]. Measurement sites were defined as follows: (a) 2.5 cm laterally between L3 and L4 spinous processes for erector spinae 1 indicated superficial erector spinae muscles, (b) 7 cm laterally from the L3 spinous process of erector spinae 2 indicated deep erector spinae muscles, and (c) 2 cm laterally to the L4 spinous process for the multifidus (Figure 1) [24,25]. Measurement postures for data collection in the prone posture were performed on the flat and the Wilson table (Figure 2). Before ultrasound image collection, each spinous process of the lumbar spine was palpated and marked to ensure that ultrasound images were captured at the correct position. At each posture, each subject was asked to relax. Then, five SWE images of the lumbar erector spinae and multifidus muscles were collected.

Each shear elastic modulus of the aforementioned muscles was evaluated by measuring shear-wave propagation speed in the tissue, which was generated using SWE at each measurement posture. The circular regions of interest (ROIs) were set in the color-coded boxes on the SWE mode (Figure 3). Three circular ROIs with a diameter of 10 mm were set in the color-coded box, with one located at the top-center of the box and the other two located at the inferior to the first-assigned circular ROI (Figure 3) [21,24]. Shear elastic modulus at the set ROI was automatically calculated from the ultrasound imaging device. The mean shear-elastic-modulus values of the three circular ROIs were calculated for each muscle per posture for five images. ROIs were determined by the same examiner.

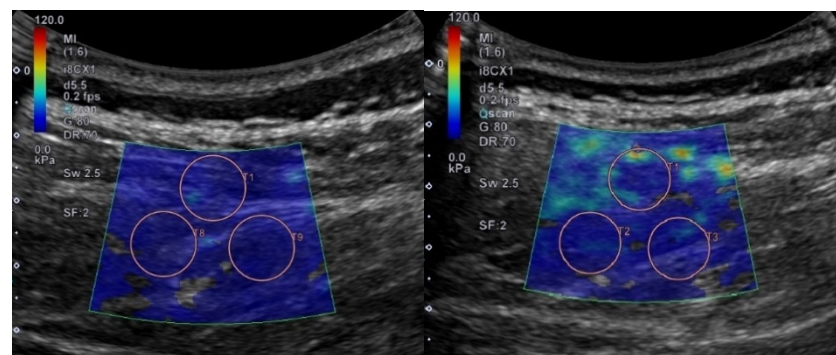


(a)



(b)

Figure 2. Two different prone postures on (a) flat table and (b) Wilson table.



(a)

(b)

Figure 3. Example for setting regions of interest to measure shear elastic modulus in different postures on flat and Wilson table. In this case, erector spinae 1 located at L3–4 is shown: (a) flat table; (b) Wilson table.

Skin and muscle thicknesses were measured from the collected shear-wave ultrasound images using Image J 1.52a (National Institutes of Health, Bethesda, U.S.). Skin thickness was measured as the distance (cm) between the surface of the epidermis and the subcutaneous tissue. Muscle thickness was measured as the distance between superficial and deep muscle fascias. Both skin and muscle thicknesses were measured by drawing a straight line through the center of the image [26] (Figure 4). Skin and muscle thicknesses were measured using one shear-wave ultrasound image per muscle and condition.

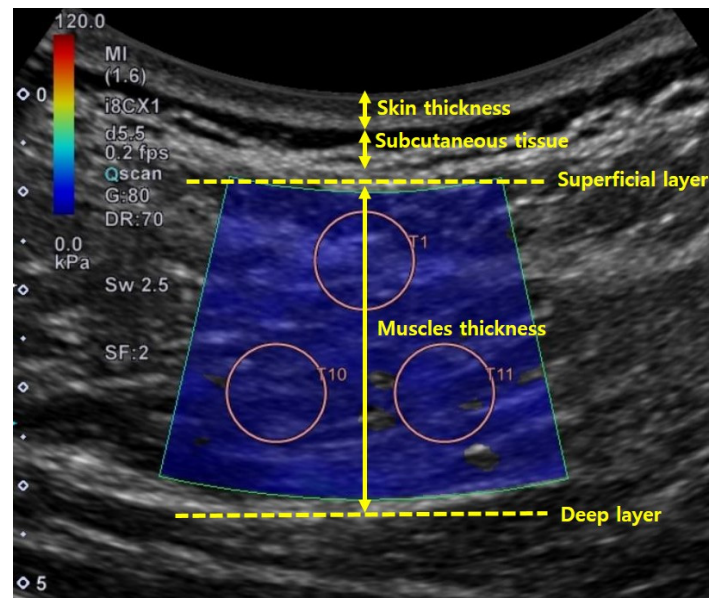


**Figure 4.** Method used to determine skin and muscle thicknesses in ultrasound image.

#### 2.4. Statistics

Data normality at each condition was checked using a Jarque–Bera test. Spinal-alignment and muscle-thickness measurements were not normally distributed. Skin thickness and muscle shear-elastic-modulus measures were normally distributed. Thereby, Wilcoxon signed-rank tests were used to compare the values between flat and Wilson table to determine spinal alignment at T1, T12, and L5, and the muscle thickness of erector spinae 1, erector spinae 2, and multifidus. Paired *t*-tests were used to compare the values between the flat and the Wilson table to determine the skin thickness and shear elastic modulus from the erector spinae 1, erector spinae 2, and multifidus. The effect size of the significant condition was also reported. A two-way repeated-measures analysis of variance (ANOVA) test was performed to investigate whether different muscles and postures showed differences in muscle shear-elastic-modulus measures. Independent variables were muscle and posture, and posture was repeated. Post hoc analysis with Bonferroni correction was performed to investigate which muscle pairs showed significant differences; thus, *p* value was adjusted by multiplying by 3. The average intraclass correlation coefficient (ICC) of the shear elastic modulus was also investigated using five images of each muscle and posture. Because the muscle-thickness measure was not normally distributed, correlation analysis was conducted using Spearman’s correlation tests for the factors of skin thickness, muscle thickness, and shear elastic modulus of each muscle. *p* values less than 0.05 were considered statistically significant.

### 3. Results

#### 3.1. Spinal Alignment

Wilcoxon signed-rank tests revealed that thoracic curvature angles at T1 ( $p = 0.001$ , effect size:  $r = -0.62$ ) and the lumbar curvature angle at L5 ( $p = 0.001$ , effect size:  $r = -0.62$ )

were significantly different between postures (Figure 5). The thoracic curvature angle at T12 was not significantly different between postures.

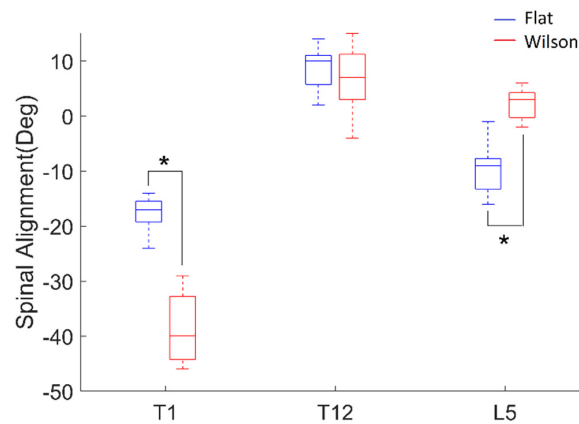


**Figure 5.** Spinal alignment (deg) of thoracic curvature angle at T1 and T12, and lumbar curvature angles at L5 from postures on flat (blue) and Wilson (red) tables. Each box plot indicates 25th (Q1), 50th (Q2), and 75th (Q3) data percentiles. Whisker indicates  $Q3 + 1.5 \times (Q3 - Q1)$  and  $Q1 - 1.5 \times (Q3 - Q1)$ . \*,  $p < 0.05$ .

### 3.2. Skin and Muscle Thickness

Paired *t*-tests revealed that skin thicknesses in the sites used to measure the erector spinae 2 ( $p = 0.007$ , effect size:  $d = 0.90$ ) and multifidus ( $p = 0.006$ , effect size:  $d = 0.93$ ) muscles showed significant differences between flat and Wilson table (Figure 6). However, the skin thickness of the site used to measure erector spinae 1 was not statistically different between the flat and Wilson table. Wilcoxon signed-rank tests revealed that the muscle thicknesses of erector spinae 1 ( $p = 0.001$ , effect size:  $r = -0.62$ ), erector spinae 2 ( $p = 0.003$ , effect size:  $r = -0.58$ ), and multifidus ( $p = 0.039$ , effect size:  $r = -0.40$ ) muscles showed significant differences between flat and Wilson table.

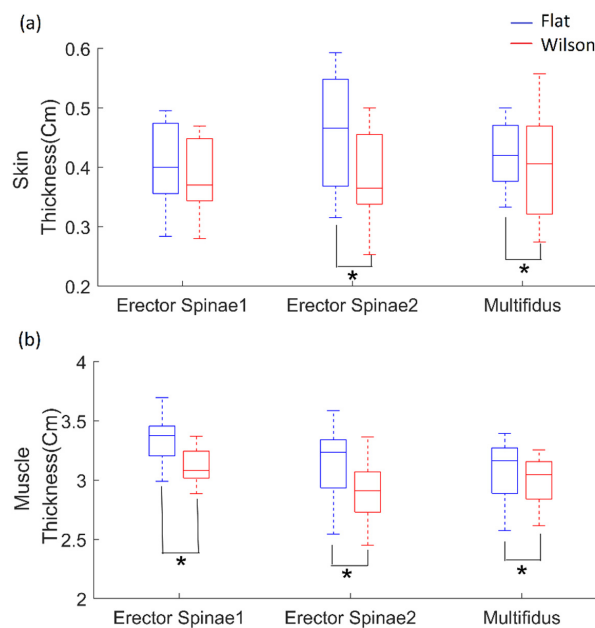


**Figure 6.** (a) Skin thickness in sites used to measure erector spinae 1 and 2, and multifidus; (b) muscle thickness based on flat (blue) and Wilson (red) table postures. Each box plot indicates 25th (Q1), 50th (Q2), and 75th (Q3) data percentiles. Whisker indicates  $Q3 + 1.5 \times (Q3 - Q1)$  and  $Q1 - 1.5 \times (Q3 - Q1)$ . \*,  $p < 0.05$ .

### 3.3. Shear Elastic Modulus

Paired *t*-tests revealed that the shear modulus of erector spinae 1 ( $p < 0.001$ , effect size:  $d = -2.13$ ), erector spinae 2 ( $p < 0.001$ , effect size:  $d = -1.72$ ), and multifidus ( $p < 0.001$ , effect size:  $d = -1.96$ ) muscles significantly increased from flat table to Wilson table posture (Figure 7). Two-way ANOVA revealed that posture ( $p < 0.001$ ), muscle ( $p < 0.001$ ), and interactions between posture and muscle ( $p = 0.001$ ) had a significant effect. Post hoc analysis with Bonferroni correction revealed that there were significant differences in the shear-modulus value between erector spinae 1 and 2 ( $p < 0.001$ ), and erector spinae 2 and multifidus ( $p = 0.002$ ). The mean ICC value of erector spinae 1 in the flat posture was 0.942, and that in the Wilson table posture was 0.842. The mean ICC value of the erector spinae 2 in the flat posture was 0.878, and that in the Wilson posture was 0.903. The mean ICC value of the multifidus in the flat posture was 0.840, and that in the Wilson table posture was 0.805.

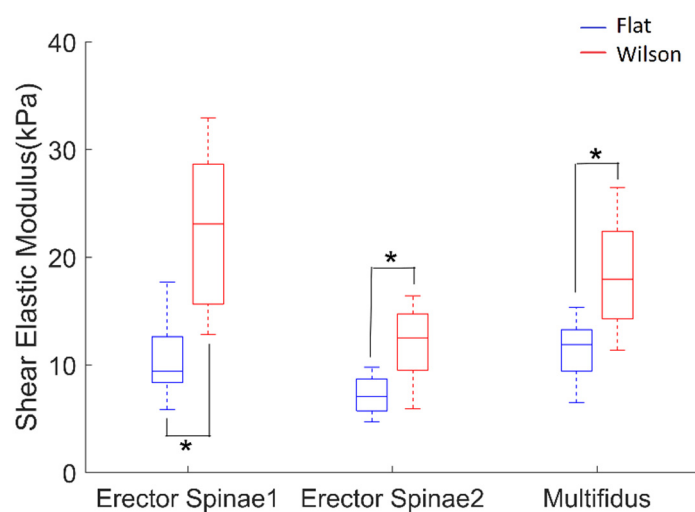


**Figure 7.** Shear elastic modulus of erector spinae 1, erector spinae 2, and multifidus muscles while in flat (blue) and Wilson (red) table postures. Each box plot indicates 25th (Q1), 50th (Q2), and 75th (Q3) percentiles of the data. Whisker indicates  $Q3 + 1.5 \times (Q3 - Q1)$  and  $Q1 - 1.5 \times (Q3 - Q1)$ . \*,  $p < 0.05$ .

### 3.4. Correlation between Muscle Thickness, Skin Thickness, and Shear Elastic Modulus

There was significant negative correlation between the muscle thickness and shear elastic modulus of erector spinae 1 ( $p = 0.044$ ,  $\rho = -0.398$ ), erector spinae 2 ( $p = 0.024$ ,  $\rho = -0.443$ ), and multifidus ( $p = 0.040$ ,  $\rho = -0.405$ ). There was also significant negative correlation between the skin thickness and shear elastic modulus of the multifidus ( $p = 0.047$ ,  $\rho = -0.393$ ).

## 4. Discussion

In this study, the skin thickness, muscle thickness, and shear elastic modulus of muscles around the lumbar spine in a spinal-surgery prone position on a Wilson table were investigated. Our hypotheses supported our findings that there were significant differences in the shear elastic moduli of the erector spinae and multifidus muscles between the flat and Wilson table postures. Posture was also found to have significant effects on muscle and skin thickness. Significant negative correlations were found between muscle thickness and shear elastic modulus of all muscles.

Significantly higher shear elastic moduli in all test muscles (superficial and deep erector spinae muscles and the multifidus muscle) were found in the Wilson table condition compared to the flat-table condition. Significantly higher shear elastic moduli indicate that muscles became stiffer when they were on the Wilson table compared to the flat table. Elastography is a method used to characterize tissue mechanical structure and material

properties. Furthermore, SWE monitors changes in tissue acoustic impedance properties through the propagation of shear waves [27,28]. Because both the erector spinae and lumbar multifidus muscles have roles in trunk ipsilateral flexion [21], the elongation of muscles caused by the Wilson table could be reflected by increases in the shear elastic moduli of erector spinae and lumbar multifidus muscles. Significant differences in spinal alignments at T1 and L5, but not at T12, between postures are related to spinal curvature changes caused by the Wilson table compared to the flat table (Figure 1). On the basis of our findings, spinal alignments at T12 were not necessarily changed due to the Wilson table. Such changes in spinal curvature have an impact on the elongation of the lumbar muscles, such as the erector spinae and multifidus. Therefore, significantly higher shear elastic modulus could be found in all test muscles.

Our results are also supported by a previous study that compared shear elastic modulus across various trunk positions for developing stretching-based rehabilitation therapy [21]. In the study, significantly higher shear elastic moduli of the erector spinae muscle in the flexion–lateral flexion position were found compared to the rest or flexion positions, while a similar shear elastic modulus in the multifidus muscle was found among the flexion–lateral flexion position and flexion position; however, this was significantly lower in the rest position [21]. The other study evaluated paraspinal muscle stiffness using SWE by comparing several passive and active postures in healthy individuals. Different biomechanical behaviors were detected among all paraspinal muscles, depending on changing body position [29]. In particular, multifidus muscles stiffened proportionally more than the longissimus and iliocostalis did, probably to provide stabilization for the intervertebral joints. In the passive flexion posture, where a participant is laying down on the table with a 30° angulation at the level of the anterior superior iliac spine, shear-wave velocity of the multifidus at the first sacral vertebra and the multifidus at the level of the third lumbar vertebra were significantly increased compared to in the rest position [29]. In accordance with previous works, in this study, the shear elastic modulus between the two postures among muscles was different. This may have been due to the location of the muscles, where erector spinae 1 is the most superficial muscle compared to the erector spinae 2 and multifidus muscles. The erector spinae muscle is a member of the superficial muscles of the trunk and has a long extension moment arm (MA) for the trunk, at  $6.1 \pm 0.6$  cm in the extension direction, and at  $2.2 \pm 0.4$  cm in the ipsilateral lateral flexion direction [21,30]. However, the multifidus muscle is a member of the deep muscles of the trunk and has a shorter MA compared to the erector spinae muscles, at  $5.5 \pm 0.7$  cm in the extension MA and  $1.1 \pm 0.1$  cm in the ipsilateral lateral flexion MA [21,30]. Considering that a previous study found a more stretched muscle-tendon unit when the change in joint angle was higher or muscle MA was longer [31], a higher shear modulus on the Wilson table compared to the flat table may be due to a change in the joint angle, but a greater change in the superficial muscle is due to the longer MA leading to more muscle stretch.

Muscle elasticity can be influenced by many factors, such as physiological status, anesthesia status, and the use or non-use of muscle relaxants in consideration of clinical applications of the current findings. Due to a lack of studies associated with the assessment of material parameters in muscles under anesthetic conditions, it is uncertain how muscle relaxants and anesthesia would influence our results. Clinically, we determined that there are no differences between skeletal-muscle tone during general anesthesia with and without a muscle relaxant on spinal-surgery patients [32]. Isometric skeletal-muscle strength during general and spinal anesthesia was observed in humans. Using clinically applicable doses of bupivacaine, muscle strength was decreased by about 20%, whereas under general anesthesia (propofol and sevoflurane), muscle strength remained unchanged [33]. Additionally, the different effects of propofol, ketamine, and thiopental anesthesia on dorsal striated muscle microcirculation were observed in rats. The administration of thiopental and propofol induced the dilatation of arterioles and venules, but ketamine had the opposite effect at the induction period [34]. Depending on concentration, the same drug demonstrated different effects; in particular, thiopental demonstrated dose-dependent

microvascular constriction [35]. Thus, the material properties of skeletal muscles during anesthesia could be different from those in the relaxed condition in our study. As such, this requires further investigation.

Although this is the first study comparing the shear moduli of the erector spinae and lumbar multifidus muscles between flat and Wilson table conditions, few studies investigated the moduli of the erector spinae and lumbar multifidus muscles [21,24,36–40]. Our shear-modulus values for erector spinae 1, erector spinae 2, and multifidus muscles in the flat-table condition were comparable with those of previous studies in the range of approximately 14–18 kPa [36–39]. There is a study that reported lower values than ours, between 5–7 kPa in the multifidus muscle [40]. SWE values can be influenced by transducer type (either linear or convex probes), the frequency of image acquisition, the angle between transducer and muscle fibers, and ROI location in the images [41]. In our case, the different values from a previous study may have come from the angle between transducer and muscle fibers since stiffness values are greater in the parallel direction rather than perpendicular to the muscle fibers [40]. Furthermore, the applied pressure to the ultrasound probe could influence the shear-elastic-modulus value [42]. Overall, our values and findings are reasonable and can be justified. Furthermore, they are supported by our good ICC values in shear elastic modulus from 0.805 to 0.942. Since all subjects were healthy males, further studies comparing gender differences and differences due to pathological conditions could be interesting to pursue. A previous study [12] revealed that, during miniature robotic guidance for spine surgery on the clinical side, too much force to the tool guide applied by the surgeon and excessive pressure on the robotic guide arm caused by the surrounding soft tissue could cause a deviation from the preoperative surgical plan. Thereby, changes in the muscle moduli depending on posture and subject characteristics could have an impact on the surgical plan. Only using image-to-patient registration technologies such as the paired-point method might not address this issue.

## 5. Conclusions

In our findings, the Wilson table posture had an impact on muscle elastic properties compared to the resting posture. As such, surgical instrument and position might better inform surgical training and planning. By considering muscle and soft-tissue properties on the basis of the surgical position, more reliable robotics-aided spinal surgeries can be realized in the future. Furthermore, including these properties in a biomechanical model could assist with surgical training and planning for surgical procedures using MIMA.

**Author Contributions:** Conceptualization, T.H.L., D.L., and S.J.L.; methodology, S.J.L.; software, S.J.L.; validation, T.H.L., O.K., D.L., and S.J.L.; formal analysis, T.H.L., O.K., D.L., and S.J.L.; investigation, T.H.L., O.K., D.L., and S.J.L.; resources, D.L.; data curation, T.H.L., and S.J.L.; writing—original-draft preparation, T.H.L., O.K., D.L., and S.J.L.; writing—review and editing, T.H.L., O.K., D.L., and S.J.L.; visualization, O.K., and S.J.L.; supervision, S.J.L.; project administration, D.L.; funding acquisition, D.L., and S.J.L. All authors have read and agreed to the published version of the manuscript.

**Funding:** This research was supported in part by the WC300 project funded by Korea Institute for Advancement of Technology (KIAT), S2482672, and by the National Research Foundation of Korea (NRF) grant funded by the Korea Government (MSIT), no. 2020R1C1C1005084.

**Institutional Review Board Statement:** The study was conducted according to the guidelines of the Declaration of Helsinki, and approved by the Institutional Review Board of Korea Institute of Science and Technology (2019-034 and 2019.10.08).

**Informed Consent Statement:** Informed consent was obtained from all subjects involved in the study.

**Data Availability Statement:** The data presented in this study are available on request from the corresponding author.

**Conflicts of Interest:** The authors declare no conflict of interest.

## References

1. Lebl, D.R. Minimally Invasive Spine Surgery. *Curr. Rev. Musculoskelet. Med.* **2017**, *10*, 407–408. [[CrossRef](#)] [[PubMed](#)]
2. Audette, M.A.; Ferrie, F.P.; Peters, T.M. An algorithmic overview of surface registration techniques for medical imaging. *Med. Image Anal.* **2000**, *4*, 201–217. [[CrossRef](#)]
3. Holly, L.T.; Bloch, O.; Johnson, J.P. Evaluation of registration techniques for spinal image guidance. *J. Neurosurg. Spine* **2006**, *4*, 323–328. [[CrossRef](#)] [[PubMed](#)]
4. Wyawahare, M.; Patil, P.; Abhyankar, H. Image Registration Techniques: An overview. *Image Process. Pattern Recognit.* **2009**, *2*, 11–28.
5. Kochanski, R.B.; Lombardi, J.M.; Laratta, J.L.; Lehman, R.A.; O’Toole, J.E. Image-Guided Navigation and Robotics in Spine Surgery. *Neurosurgery* **2019**, *84*, 1179–1189. [[CrossRef](#)]
6. Tjardes, T.; Shafizadeh, S.; Rixen, D.; Paffrath, T.; Bouillon, B.; Steinhausen, E.S.; Baethis, H. Image-guided spine surgery: State of the art and future directions. *Eur. Spine J.* **2010**, *19*, 25–45. [[CrossRef](#)]
7. Elmi-Terander, A.; Skulason, H.; Soderman, M.; Racadio, J.; Homan, R.; Babic, D.; van der Vaart, N.; Nachabe, R. Surgical Navigation Technology Based on Augmented Reality and Integrated 3D Intraoperative Imaging: A Spine Cadaveric Feasibility and Accuracy Study. *Spine* **2016**, *41*, E1303–E1311. [[CrossRef](#)]
8. Gelalis, I.D.; Paschos, N.K.; Pakos, E.E.; Politis, A.N.; Arnaoutoglou, C.M.; Karageorgos, A.C.; Ploumis, A.; Xenakis, T.A. Accuracy of pedicle screw placement: A systematic review of prospective in vivo studies comparing free hand, fluoroscopy guidance and navigation techniques. *Eur. Spine J.* **2012**, *21*, 247–255. [[CrossRef](#)] [[PubMed](#)]
9. Meng, X.T.; Guan, X.F.; Zhang, H.L.; He, S.S. Computer navigation versus fluoroscopy-guided navigation for thoracic pedicle screw placement: A meta-analysis. *Neurosurg. Rev.* **2016**, *39*, 385–391. [[CrossRef](#)]
10. Perna, F.; Borghi, R.; Pilla, F.; Stefanini, N.; Mazzotti, A.; Chehrassan, M. Pedicle screw insertion techniques: An update and review of the literature. *Musculoskelet. Surg.* **2016**, *100*, 165–169. [[CrossRef](#)]
11. Huang, J.; Li, Y.; Huang, L. Spine surgical robotics: Review of the current application and disadvantages for future perspectives. *J. Robot. Surg.* **2020**, *14*, 11–16. [[CrossRef](#)] [[PubMed](#)]
12. Barzilay, Y.; Liebergall, M.; Fridlander, A.; Knoller, N. Miniature robotic guidance for spine surgery—introduction of a novel system and analysis of challenges encountered during the clinical development phase at two spine centres. *Int. J. Med. Robot. Comput. Assist. Surg.* **2006**, *2*, 146–153. [[CrossRef](#)]
13. Ringel, F.; Stuer, C.; Reinke, A.; Preuss, A.; Behr, M.; Auer, F.; Stoffel, M.; Meyer, B. Accuracy of robot-assisted placement of lumbar and sacral pedicle screws: A prospective randomized comparison to conventional freehand screw implantation. *Spine* **2012**, *37*, E496–E501. [[CrossRef](#)]
14. Lalonde, N.M.; Villemure, I.; Pannetier, R.; Parent, S.; Aubin, C.E. Biomechanical modeling of the lateral decubitus posture during corrective scoliosis surgery. *Clin. Biomech.* **2010**, *25*, 510–516. [[CrossRef](#)]
15. Fritz, M. Dynamic properties of the biomechanical model of the human body—influence of posture and direction of vibration stress. *J. Low Freq. Noise Vib. Active Control* **2005**, *24*, 233–249. [[CrossRef](#)]
16. Klausner, A.S.; Miyamoto, H.; Bellmann-Weiler, R.; Feuchtner, G.M.; Wick, M.C.; Jaschke, W.R. Sonoelastography: Musculoskeletal applications. *Radiology* **2014**, *272*, 622–633. [[CrossRef](#)] [[PubMed](#)]
17. Taljanovic, M.S.; Gimber, L.H.; Becker, G.W.; Latt, L.D.; Klausner, A.S.; Melville, D.M.; Gao, L.; Witte, R.S. Shear-Wave Elastography: Basic Physics and Musculoskeletal Applications. *Radiographics* **2017**, *37*, 855–870. [[CrossRef](#)] [[PubMed](#)]
18. Arda, K.; Ciledag, N.; Aktas, E.; Aribas, B.K.; Kose, K. Quantitative Assessment of Normal Soft-Tissue Elasticity Using Shear-Wave Ultrasound Elastography. *Am. J. Roentgenol.* **2011**, *197*, 532–536. [[CrossRef](#)]
19. Chino, K.; Akagi, R.; Dohi, M.; Fukushima, S.; Takahashi, H. Reliability and validity of quantifying absolute muscle hardness using ultrasound elastography. *PLoS ONE* **2012**, *7*, e45764. [[CrossRef](#)]
20. Chino, K.; Akagi, R.; Dohi, M.; Takahashi, H. Measurement of muscle architecture concurrently with muscle hardness using ultrasound strain elastography. *Acta Radiol.* **2014**, *55*, 833–839. [[CrossRef](#)]
21. Masaki, M.; Ji, X.; Yamauchi, T.; Tateuchi, H.; Ichihashi, N. Effects of the trunk position on muscle stiffness that reflects elongation of the lumbar erector spinae and multifidus muscles: An ultrasonic shear wave elastography study. *Eur. J. Appl. Physiol.* **2019**, *119*, 1085–1091. [[CrossRef](#)]
22. Lee, S.J.; Ren, Y.; Kang, S.H.; Geiger, F.; Zhang, L.Q. Pivoting neuromuscular control and proprioception in females and males. *Eur. J. Appl. Physiol.* **2015**, *115*, 775–784. [[CrossRef](#)] [[PubMed](#)]
23. Stokes, M.; Rankin, G.; Newham, D.J. Ultrasound imaging of lumbar multifidus muscle: Normal reference ranges for measurements and practical guidance on the technique. *Man. Ther.* **2005**, *10*, 116–126. [[CrossRef](#)]
24. Masaki, M.; Aoyama, T.; Murakami, T.; Yanase, K.; Ji, X.; Tateuchi, H.; Ichihashi, N. Association of low back pain with muscle stiffness and muscle mass of the lumbar back muscles, and sagittal spinal alignment in young and middle-aged medical workers. *Clin. Biomech.* **2017**, *49*, 128–133. [[CrossRef](#)] [[PubMed](#)]
25. Wong, A.Y.; Parent, E.C.; Kawchuk, G.N. Reliability of 2 ultrasonic imaging analysis methods in quantifying lumbar multifidus thickness. *J. Orthop. Sports Phys. Ther.* **2013**, *43*, 251–262. [[CrossRef](#)]
26. Gibbon, K.C.; Debusse, D.; Hibbs, A.; Caplan, N. Reliability and Precision of Sonography of the Lumbar Multifidus and Transversus Abdominis During Dynamic Activities. *J. Ultrasound Med.* **2017**, *36*, 571–581. [[CrossRef](#)] [[PubMed](#)]

27. Rasool, G.; Wang, A.B.; Rymer, W.Z.; Lee, S.S.M. Shear Waves Reveal Viscoelastic Changes in Skeletal Muscles After Hemispheric Stroke. *IEEE Trans. Neural. Syst. Rehabil. Eng.* **2018**, *26*, 2006–2014. [[CrossRef](#)]
28. Sarvazyan, A.; Hall, T.J.; Urban, M.W.; Fatemi, M.; Aglyamov, S.R.; Garra, B.S. An Overview of Elastography—An Emerging Branch of Medical Imaging. *Curr. Med. Imaging Rev.* **2011**, *7*, 255–282. [[CrossRef](#)]
29. Creze, M.; Bedretdinova, D.; Soubeyrand, M.; Rocher, L.; Gennisson, J.L.; Gagey, O.; Maitre, X.; Bellin, M.F. Posture-related stiffness mapping of paraspinal muscles. *J. Anat.* **2019**, *234*, 787–799. [[CrossRef](#)]
30. McGill, S.M.; Santaguida, L.; Stevens, J. Measurement of the Trunk Musculature from T5 to L5 Using Mri Scans of 15 Young Males Corrected for Muscle-Fiber Orientation. *Clin. Biomech.* **1993**, *8*, 171–178. [[CrossRef](#)]
31. Maganaris, C.N.; Baltzopoulos, V.; Sargeant, A.J. In vivo measurement-based estimations of the human Achilles tendon moment arm. *Eur. J. Appl. Physiol.* **2000**, *83*, 363–369. [[CrossRef](#)]
32. Li, Y. The Effects of Neuromuscular Blockade on Operating Conditions During General Anesthesia for Spinal Surgery. *J. Neurosurg. Anesthesiol.* **2014**, *26*, 45–49. [[CrossRef](#)]
33. Ginz, H.F.; Zorzato, F.; Iaizzo, P.A.; Urwyler, A. Effect of three anaesthetic techniques on isometric skeletal muscle strength. *Br. J. Anaesth.* **2004**, *92*, 367–372. [[CrossRef](#)]
34. Brookes, Z.L.; Brown, N.J.; Reilly, C.S. Intravenous anaesthesia and the rat microcirculation: The dorsal microcirculatory chamber. *Br. J. Anaesth.* **2000**, *85*, 901–903. [[CrossRef](#)]
35. Brookes, Z.L.; Reilly, C.S.; Brown, N.J. Differential effects of propofol, ketamine, and thiopental anaesthesia on the skeletal muscle microcirculation of normotensive and hypertensive rats in vivo. *Br. J. Anaesth.* **2004**, *93*, 249–256. [[CrossRef](#)]
36. Dieterich, A.V.; Andrade, R.J.; Le Sant, G.; Falla, D.; Petzke, F.; Hug, F.; Nordez, A. Shear wave elastography reveals different degrees of passive and active stiffness of the neck extensor muscles. *Eur. J. Appl. Physiol.* **2017**, *117*, 171–178. [[CrossRef](#)]
37. Alis, D.; Durmaz, E.S.M.; Alis, C.; Erol, B.C.; Okur, B.; Kizilkilic, O.; Mihmanli, I. Shear Wave Elastography of the Lumbar Multifidus Muscle in Patients With Unilateral Lumbar Disk Herniation. *J. Ultrasound Med.* **2019**, *38*, 1695–1703. [[CrossRef](#)] [[PubMed](#)]
38. Chan, S.T.; Fung, P.K.; Ng, N.Y.; Ngan, T.L.; Chong, M.Y.; Tang, C.N.; He, J.F.; Zheng, Y.P. Dynamic changes of elasticity, cross-sectional area, and fat infiltration of multifidus at different postures in men with chronic low back pain. *Spine J.* **2012**, *12*, 381–388. [[CrossRef](#)] [[PubMed](#)]
39. Moreau, B.; Vergari, C.; Gad, H.; Sandoz, B.; Skalli, W.; Laporte, S. Non-invasive assessment of human multifidus muscle stiffness using ultrasound shear wave elastography: A feasibility study. *Proc. Inst. Mech. Eng. Part H J. Eng. Med.* **2016**, *230*, 809–814. [[CrossRef](#)] [[PubMed](#)]
40. Creze, M.; Timoh, K.N.; Gagey, O.; Rocher, L.; Bellin, M.F.; Soubeyrand, M. Feasibility assessment of shear wave elastography to lumbar back muscles: A Radioanatomic Study. *Clin. Anat.* **2017**, *30*, 774–780. [[CrossRef](#)]
41. Sadeghi, S.; Quinlan, K.; Eilertson, K.E.; Billy, G.G.; Bible, J.; Sions, J.M.; Cortes, D.H. Changes in Shear Modulus of the Lumbar Multifidus Muscle During Different Body Positions. *J. Biomech. Eng.* **2019**, *141*. [[CrossRef](#)] [[PubMed](#)]
42. Kot, B.C.; Zhang, Z.J.; Lee, A.W.; Leung, V.Y.; Fu, S.N. Elastic modulus of muscle and tendon with shear wave ultrasound elastography: Variations with different technical settings. *PLoS ONE* **2012**, *7*, e44348. [[CrossRef](#)] [[PubMed](#)]